Link Loss Analysis of Integrated Linear Weight Bank within Silicon Photonic Neural Network

Eric C. Blow^{a,b}, Jiawei Zhang^b, Weipeng Zhang^b, Simon Bilodeau^b, Josh Lederman^b, Bhavin Shastri^c, and Paul R. Prucnal^b

aNEC Laboratories America Inc, 4 Independence Way, Princeton, NJ 08540
 bPrinceton University, Engineering Quadrangle, Princeton, NJ 08540
 cQueen's University, Department of Physics, Engineering Physics & Astronomy, Queen's University, Kingston, Ontario, Canada, K7M 3N6

ABSTRACT

In the past decade, the field of neuromorphic photonics has experienced significant growth. To extend the reach of this technology, researchers continue to push the limits of these systems with respect to network size and bandwidth. However, without proper RF-optimized architectural designs, as operating frequencies are scaled up, significant losses of RF power can be incurred at each neuron. Within the broadcast and weight neuromorphic photonic architecture, this excess loss will be accumulated until processing is no longer feasible. If designed properly, RF loss can be minimized significantly, and residual loss could be compensated by cointegrated transimpedance amplifiers, thus enabling further scaling of the network. In this paper, the authors present broadband weighting of RF input signals with a 3-dB bandwidth of 4.28 GHz, utilizing the linear frontend of a silicon photonic neural network. Additionally, the authors present link loss measurements and analysis.

Keywords: Neuromorphic Photonics, RF Photonics, Silicon Photonics. Broadband Analog Processing

1. INTRODUCTION

Neuromorphic photonic systems leverage the analog processing benefits of integrated microwave photonics, ¹ such as high bandwidth, low latency, and high dynamic range, when applied to machine learning (ML) processing tasks. ² This technique enables the generation of ML insights, such as classification, on GHz radio frequency (RF) wireless signals in near-real time. ^{3,4} The superior bandwidth and latency performance offered by neuromorphic photonics would not be possible using conventional microelectronic processors. ²

However, this technological approach has experienced a limited application space due to the small neural network size.⁵ When scaling the size of photonic nueral network (PNNs), the degradation of the signal-to-noise ratio (SNR) must be considered as a function of network depth, the number of layers. As shown by Ferriera de Lima, et. al.,⁶ the nonlinear processing within the photonic neural network preserves the noise performance from layer to layer but the signal power degrades due to inefficiencies within the photonic link. Historically, the RF power loss incurred in an analog photonic link, known as the link loss, is very high, typically ~40 dB.⁷ With such a high link loss, scaling the PNNs would require transimpedance amplification (TIA) between the neuron layers of 40 dB, which is unrealistic for a co-integrated amplifier. Within this paper, the link loss of current linear front-end designs is simulated and measured to serve as a benchmark. The previous work from Blow et al. investigates the performance of previous PNN architectures, as well as providing analysis on additional RF metrics not discussed in this paper.^{8,9}

Send correspondence to E.C.B.: E-mail: blow@nec-labs.com

2. LINEAR ON-CHIP LINEAR WEIGHTING

Within broadcast and weight PNN architectures, Microring Resonators (MRRs) and Balanced Photodetectors (BPDs) are implemented together in a weight bank configuration to achieve weighted summation, the linear processing requirement of an artificial neuron. The 8 µm ring has spectral resonances at integer multiple of the ring's circumference. At these wavelengths, optical carriers coupled into the ring constructively interfere after circulating and optical power builds within the ring. This optical power is then coupled into the drop waveguide. If off-resonance the light will fail to constructively interfere and therefore will remain on the input bus waveguide, known as the through port. In a weight bank, the through and port are terminated by a balanced photodetector, at which each photodetector sums all modulated signals regardless of wavelength and then outputs the differential current between photodetectors, enabling both positive and negative weighting. Additionally, embedded heaters tune the MRR's resonance allowing for a continuous weighting between +1 and -1. This configuration is shown in the experimental schematic, Fig. 1c, and the micrograph of the integrated photonic chip, Fig. 1a.

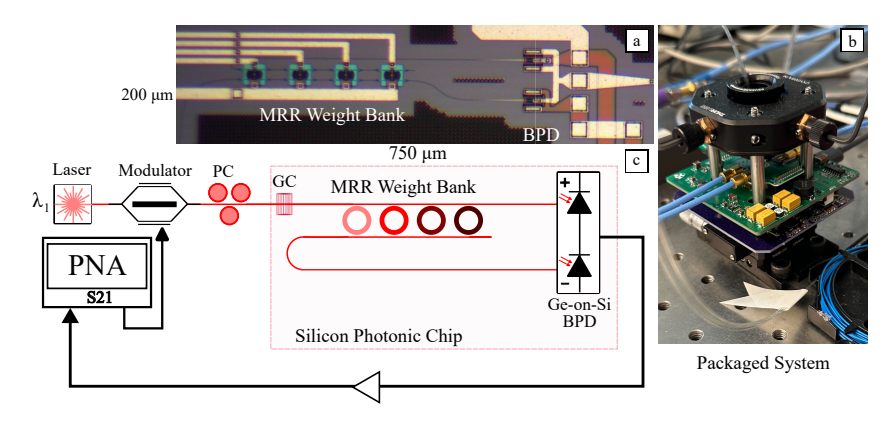


Figure 1. a) Micrograph of 200 μm by 750 μm area of a silicon photonic chip including Microring Resonator (MRR) weight bank and Germanium-on-Silicon Balanced Photodetector (BPD). b) Packaged system including vertical optical coupling, co-packaged electrical control and RF I/O. c) Experimental system diagram of linear optical weighting. PNA: Portable Network Analyzer, PC: Polarization Controller, GC: Grating Coupler

The RF weighting response of the integrated silicon neural network linear front-end is measured using a Portable Network Analyzer (PNA), N52222A. The input RF signal is modulated onto a 1542 nm optical carrier using an off-chip 10 GHz Mach-Zehnder Modulator with insertion loss of 6 dB and V_{π} of 6.7 V. The modulated optical signal is then vertically coupled onto the chip via a 6-dB loss grating coupler. The optical signal is then weighted by the on-chip weight bank and detected via the balanced photodetector, ¹³ which has a responsivity of 1.09 A/W. The electrical output signal is then amplified by an off-chip electrical amplifier with gain of 16.1 dB and noise figure of 2.5 dB. The resulting weighting of the integrated chip is significantly broadband, with a 3-dB bandwidth of 4.28 GHz referenced at 1.41 GHz, Fig 3a. The difference between the weighting transfer functions at varying weighting values is measured to calculate the weight variation as a function of frequency, Fig. 3b. This measurement highlights the possible instantaneous bandwidth of the system. The variation is low, < 0.1dB, below 4 GHz, and then high, up to 1 dB, above this cutoff. This increase in weighting variation is due to improper phase matching of the on-chip weight bank resulting in imprecise subtraction between the two optical paths. Unlike previous architectures, in which off-chip detection allowed for off-chip optical delay and phase matching.^{9,14} This implementation of the fully integrated weight bank was not designed with additional on-chip processing elements for delay and phase matching and is therefore fundamentally limited in weighting bandwidth. Lastly, the RF weighting value is also measured as a function of sweeping the MRR weighting current from 0.0 mA to 1.5 mA, Fig. 3c, for four discrete operating frequencies to highlight the effects of the MRR resonance and potential asymmetries.

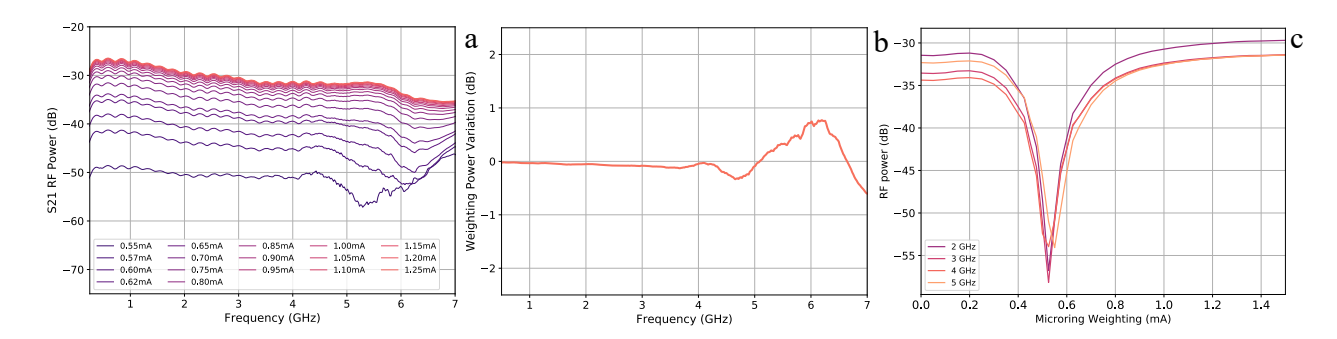


Figure 2. a) Measured S21 (dB) of on-chip photonic linear front end from 10 MHz to 7 GHz. S21 measured as a function of applied weighting current, swept from 0.55 mA (purple) to 1.25 mA (orange). b) Measured variation (dB) in weighting as function of frequency. c) S21 as function of applied weighting current from 0.0 mA to 1.5 mA for four well-matched single frequency points (2,3,4,5 GHz).

3. RF LINK LOSS OF LINEAR FRONT-END

Historically, the RF power loss, link loss, has been a significant cavaet to analog photonic processing.¹⁵ The link loss of an analog photonic link is dependent on four primary mechanisms: impedance matching, modulation efficiency, loss of optical processing, and detection efficiency. The system presented is passively impedance matched to maximize bandwidth and therefore a 1/4 loss is incurred.⁷ The presented system is externally modulated and therefore the gain of the system depends on optical power, P_{opt} , insertion loss of the modulator, T_{mod} , the load resistance, R_L , and the sensitivity of the modulator, V_{π} . The loss of optical processing includes the insertion loss of the ring, 0.2 dB, the coupling loss, 6 dB, linear propagation loss of the waveguide, 1.04 dB/cm, ¹⁶ and the nonlinear loss within the waveguide and MRR. ^{17–19}

$$G_{\text{PNN}} = \left(G_{\text{Impedance}}\right) \left(G_{\text{mod}}\right)^2 \left(G_{\text{opt}}\right)^2 \left(G_{\text{Detect}}\right)^2 \tag{1}$$

$$G_{\text{PNN}} = (1/4) \left(\frac{P_{\text{opt}} T_{\text{Mod}} R_L \pi}{2V_{\pi}} \right)^2 (G_{\text{opt}})^2 (r_{\text{PD}})^2$$
(2)

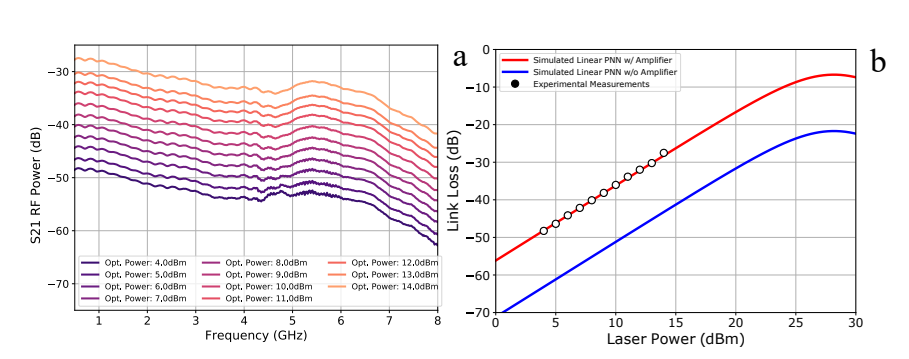


Figure 3. a) Measured S21 of analog photonic link of photonic neural network front-end as function sweeping optical power from 4 dBm to 14 dBm. b) Link loss of analog photonic link (dB) as function of optical power. Simulated RF link loss (red trace) and measured link loss at 1 GHz (white marker with black outline) match well.

The link loss of the system without electrical amplification at 1 GHz is -44 dB with 14 dBm optical power, shown in Fig. 3a. The link loss of the systems is measured while the optical power is swept into the off-chip modulator from 4 dBm (purple trace) to 14 dBm (orange trace). The resulting RF link loss is plotted as a function of optical power and showed a high match to the expected loss, the red curve. Due to the high loss of the modulator and the coupling into the photonic integrated circuit, nonlinear effects within the waveguides and MRR are not observed to be significant until much higher optical powers, 25 dB. With a low insertion loss

modulator, 4 dB, and high-quality edge coupling, 1.2 dB, ¹⁶ an 11.2 dB improvement of RF gain is expected. While lowering the optical loss of the modulator and improving coupling efficiencies will improve performance, the increase in optical power into the silicon waveguide will subsequently shift the optical power point in which nonlinear loss begins to dominate lower.

REFERENCES

- [1] Marpaung, D., Yao, J., and Capmany, J., "Integrated microwave photonics," *Nature Photonics* **13**(2), 80–90 (2019).
- [2] Prucnal, P. R. and Shastri, B. J., [Neuromorphic photonics], CRC press (2017).
- [3] Peng, H.-T., Lederman, J. C., Xu, L., De Lima, T. F., Huang, C., Shastri, B. J., Rosenbluth, D., and Prucnal, P. R., "A photonics-inspired compact network: Toward real-time ai processing in communication systems," *IEEE Journal of Selected Topics in Quantum Electronics* **28**(4), 1–17 (2022).
- [4] Shastri, B. J., Tait, A. N., Ferreira de Lima, T., Pernice, W. H., Bhaskaran, H., Wright, C. D., and Prucnal, P. R., "Photonics for artificial intelligence and neuromorphic computing," *Nature Photonics* 15(2), 102–114 (2021).
- [5] Huang, C., Fujisawa, S., Ferreira de Lima, T., Tait, A. N., Blow, E. C., Tian, Y., Bilodeau, S., Jha, A., Yaman, F., Peng, H.-T., et al., "A silicon photonic–electronic neural network for fibre nonlinearity compensation," *Nature Electronics*, 1–8 (2021).
- [6] Ferreira de Lima, T., Tait, A. N., Saeidi, H., Nahmias, M. A., Peng, H.-T., Abbaslou, S., Shastri, B. J., and Prucnal, P. R., "Noise analysis of photonic modulator neurons," *IEEE Journal of Selected Topics in Quantum Electronics* 26(1), 1–9 (2020).
- [7] Cox, C. H., Ackerman, E. I., Betts, G. E., and Prince, J. L., "Limits on the performance of rf-over-fiber links and their impact on device design," *IEEE Transactions on Microwave Theory and Techniques* 54(2), 906–920 (2006).
- [8] Blow, E. C., de Lima, T. F., Peng, H.-T., Zhang, W., Huang, C., Shastri, B. J., and Prucnal, P. R., "Broadband radio-frequency signal processing with neuromorphic photonics," in [AI and Optical Data Sciences III], 12019, 157–162, SPIE (2022).
- [9] Blow, E. C., Bilodeau, S., Zhang, W., de Lima, F., Lederman, J., Thomas, Shastri, B. J., and Prucnal, P. R., "Radio-frequency linear analysis and optimization of silicon photonic neural networks," *IEEE Journal* of Selected Topics in Quantum Electronics 25(5), 1–11 (2019).
- [10] Tait, A. N., De Lima, T. F., Zhou, E., Wu, A. X., Nahmias, M. A., Shastri, B. J., and Prucnal, P. R., "Neuromorphic photonic networks using silicon photonic weight banks," *Scientific Reports* 7(1), 1–10 (2017).
- [11] Tait, A. N., Wu, A. X., De Lima, T. F., Zhou, E., Shastri, B. J., Nahmias, M. A., and Prucnal, P. R., "Microring weight banks," *IEEE Journal of Selected Topics in Quantum Electronics* **22**(6), 312–325 (2016).
- [12] Tait, A., De Lima, T. F., Nahmias, M., Shastri, B., and Prucnal, P., "Microring weight banks for neuromorphic silicon photonics," in [CLEO: Science and Innovations], STh3B–1, Optica Publishing Group (2018).
- [13] Fard, M. M. P., Cowan, G., and Liboiron-Ladouceur, O., "Responsivity optimization of a high-speed germanium-on-silicon photodetector," *Optics Express* **24**(24), 27738–27752 (2016).
- [14] Zhang, W., Tait, A., Huang, C., Ferreira de Lima, T., Bilodeau, S., Blow, E. C., Jha, A., Shastri, B. J., and Prucnal, P., "Broadband physical layer cognitive radio with an integrated photonic processor for blind source separation," *Nature Communications* 14(1), 1107 (2023).
- [15] Ackerman, E. I. and Cox, C. H., "Optimization of analog optical link performance: First minimize the noise figure," in [Microwave Photonics (MWP) and the 2014 9th Asia-Pacific Microwave Photonics Conference (APMP) 2014 International Topical Meeting on], 430–433, IEEE (2014).
- [16] Siew, S. Y., Li, B., Gao, F., Zheng, H. Y., Zhang, W., Guo, P., Xie, S. W., Song, A., Dong, B., Luo, L. W., et al., "Review of silicon photonics technology and platform development," *Journal of Lightwave Technology* 39(13), 4374–4389 (2021).
- [17] Bass, J., Tran, H., Du, W., Soref, R., and Yu, S.-Q., "Impact of nonlinear effects in si towards integrated microwave-photonic applications," *Optics Express* **29**(19), 30844–30856 (2021).

- [18] Bass, J., Brea, B., Tran, H., Du, W., Soref, R., and Yu, S.-Q., "The effect of two-photon absorption on the dynamic range of integrated microwave photonics links," in [Silicon Photonics XV], 11285, 216–223, SPIE (2020).
- [19] Tokushima, M., Ushida, J., and Nakamura, T., "Nonlinear loss characterization of continuous wave guiding in silicon wire waveguides," *Applied Physics Express* **14**(12), 122008 (2021).